Sensors & Transducers, Vol. 184, Issue 1, January 2015, pp. 116-122

Sensors & Transducers

http://www.sensorsportal.com

Error Detection on a Spectral Data Using an Optical Processor Based on a-SiC Technology

[1, 2] Manuel Augusto Vieira, [1, 2, 3] Manuela Vieira, [1, 2] Paula Louro, [1, 2] Vitor Silva

[1] Telecommunication and Computer Dept. ISEL, R. Conselheiro Emídio Navarro, 1959-007 Lisboa, Portugal
[2] CTS-UNINOVA, Quinta da Torre, Monte da Caparica, 2829-516, Caparica, Portugal
[3] DEE-FCT-UNL, Quinta da Torre, Monte da Caparica, 2829-516, Caparica, Portugal
[1] Tel.: +351218317150, fax: +351218317144
E-mail: mv@isel.ipl.pt

Received: 14 November 2014 /Accepted: 15 December 2014 /Published: 31 January 2015

Abstract In this paper, we exploit the nonlinear property of the SiC multilayer devices to design an optical processor for error detection that enables reliable delivery of spectral data of four-wave mixing over unreliable communication channels. The SiC optical processor is realized by using double pi'n/pin a-SiC:H photodetector with front and back biased optical gating elements. Visible pulsed signals are transmitted together at different bit sequences. The combined optical signal is analyzed. Data show that the background act as selector that pick one or more states by splitting portions of the input multi optical signals across the front and back photodiodes. Boolean operations such as EXOR and three bit addition are demonstrated optically, showing that when one or all of the inputs are present, the system will behave as an XOR gate representing the SUM. When two or three inputs are on, the system acts as AND gate indicating the present of the CARRY bit. Additional parity logic operations are performed using four incoming pulsed communication channels that are transmitted and checked for errors together. As a simple example of this approach, we describe an all-optical processor for error detection and then provide an experimental demonstration of this idea. *Copyright © 2015 IFSA Publishing, S. L.*

Keywords: Optical processor, Integrated optical filter, Boolean operations, Coder/decoder device, Optoelectronics.

1. Introduction

Using visible light for data transmission, which is referred to as Visible Light Communication (VLC), opens a broad spectrum of applications, such as photonic circuits for the purpose of chip-level communications and location estimation. Increases in power efficiency per bit of data are projected to be achieved by replacing electrical interconnects with their optical counterparts in the near future. Digital optical systems and optical processors demand an all-optical arithmetic unit to perform different optical arithmetic operations. Various architectures, logical and/or arithmetic operations have been proposed in optical/optoelectronic computing [1-4]. Effort has been made for the development of all-optical logical functions [5] by using different schemes like optoelectronic devices based on optical nonlinear micro-ring resonators [6-7].

Multilayered Si/C structures based on amorphous silicon technology are reconfigurable to perform WDM optoelectronic logic functions [8-9]. They

have a nonlinear magnitude-dependent response to each incident light wave. In this paper we exploit the nonlinear property of the SiC multilayer devices under steady state backgrounds to design an all-optical adder unit.

The SiC optical processor for error detection and correction is realized by using double pin/pin a-SiC:H photodetector with front and back biased optical gating elements. Red, green, blue and violet pulsed signals are transmitted together at different bit sequences. The combined optical signal is analyzed by reading out the photocurrent, under low wavelength background (350 nm) and different intensities. The operational principle of SiC based switches is discussed and the theoretical design of all-optical adder operation is reported. Experimental results confirming the described method are also presented.

After a short introduction, in Section 2, the design, characterization and operation of the device are presented. In Section 3, the spectral sensitivity of the device is analyzed and, in Section 4, the nonlinear spectral gain is presented. Section 5, refers the coder/decoder optical processor and Section 6, the full-adder design is shown. Error control methodology based on SiC technology is explained in Section 7 and the conclusions appears in Section 8.

2. Device Design, Characterization and Operation

The full-adder device is realized by using a double pi'n/pin a-SiC:H photodetector with TCO front and back biased optical gating elements as depicted in Fig. 1. The active device consists of a p-i'(a-SiC:H)-n/p-i(a-Si:H)-n heterostructure. The thicknesses and optical gap of the front i'- (200 nm; 2.1 eV) and back i- (1000 nm; 1.8 eV) layers are optimized for light absorption in the blue and red ranges, respectively [10].

Optoelectronic characterization was performed through spectral response measurements without and with steady state applied optical bias.

Monochromatic (red, green, blue and violet; $\lambda_{R,G,B,V;}$) pulsed communication channels (input channels) are combined together, each one with a specific bit sequence and absorbed accordingly their wavelengths (see arrow magnitudes in Fig. 1). The combined optical signal (multiplexed signal; MUX) is analyzed by reading out the generated photocurrent under negative applied voltage (-8 V), without and with 390 nm background lighting at different intensities, applied either from front or back sides. The device operates within the visible range using as input colour channels the square wave modulated low power light supplied by red (R: 626 nm), green (G: 524 nm), blue (B: 470 nm) and violet (V: 400 nm) LEDs.

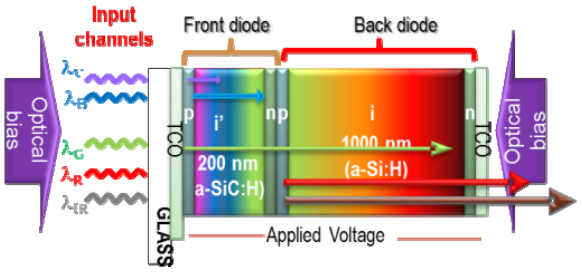

Fig. 1. Device configuration and operation.

3. Spectral Sensitivity

The spectral sensitivity was tested through spectral response measurements [11] without and under 350 nm front and back violet backgrounds using different intensities. In Fig. 2, the spectral gain (α), defined as the ratio between the spectral photocurrent with and without applied optical bias, is displayed under near-UV (λ=350 nm) illuminations. In Fig. 2a, the light was applied from the front (λ_F) and in Fig. 2b, the irradiation occurs from the back side (λ_B). The background intensity (ϕ) was changed between 5 μWcm^{-2} and 3800 μWcm^{-2}.

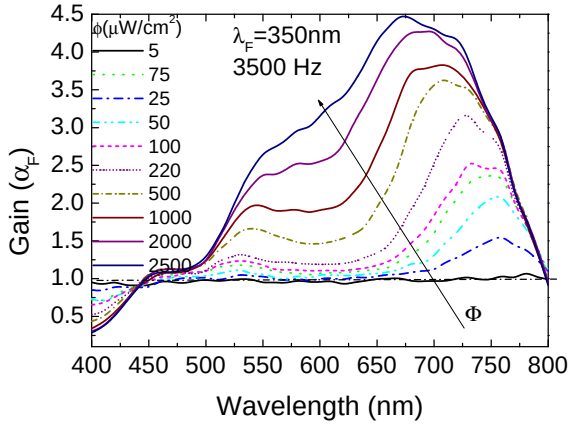

a)

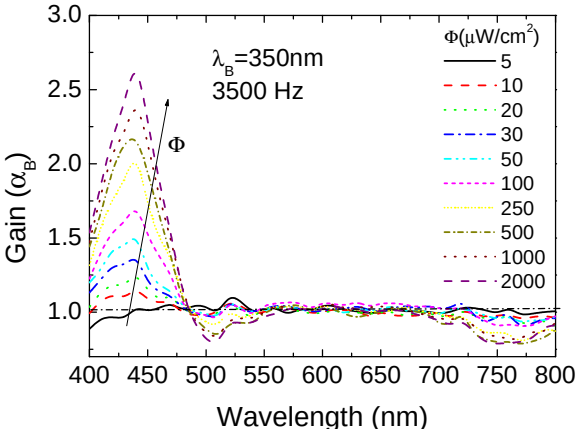

b)

Fig. 2. a) Front (λ_F) and b) back (λ_B) spectral gains ($\alpha_{F,B}$) under λ=350 nm irradiation.

Results show that the optical gains have opposite behaviours under front and back irradiations. Under 350 nm front irradiation (Fig. 2a) and low flux, the gain is high in the infrared region, presents a well-defined peak at 750 nm and strongly quenches in the visible range. As the power intensity increases the peak shifts to the visible range and can be deconvoluted into two peaks, one in the red range that slightly increases with the power density of the background and another in the green range that strongly increases with the intensity of the UV radiation. In the blue range, the gain is much lower.

This shows the controlled high-pass filtering properties of the device under different background intensities. Under back bias (Fig. 2b) the gain in the blue/violet range has a maximum near 420 nm that quickly increases with the intensity. Besides it strongly lowers for wavelengths higher than 450 nm, acting as a short-pass filter. Thus, back irradiation, tunes the violet/blue region of the visible spectrum whatever the flux intensity, while front irradiation, depending on the background intensity, selects the infrared or the visible spectral ranges.

The results show that, low fluxes select the near infrared region and cuts the visible one, the reddish part of the spectrum is selected at medium fluxes, and high fluxes tune the red/green ranges with different gains.

4. Nonlinear Optical Gains

Several monochromatic pulsed lights separately (697 nm, 626 nm, 524 nm, 470 nm, 400 nm input channels; transmitted data) or combined (MUX signal) illuminated the device at 12000 bps. Steady state 390 nm bias at different intensities due to different LED input currents ($0<I_{LED}<30$ mA) were superimposed separately from both sides and the photocurrent was measured. For each individual channel the photocurrent was normalized to its value without irradiation (dark) and the photocurrent gain ($\alpha^{V}_{R,G,B,V}$) determined. Fig. 3, displays the different gain as a function of the drive currents of the lighting LED under front (a) and back (b) irradiation.

Results show that the gain depends mainly on the channel wavelength and slightly on the lighting intensity, for high fluxes. Even across narrow bandwidths, the gains are quite different. Under front irradiation (Fig. 3a) the magnitude of the short wavelengths signals is quenched and enlarged in the long wavelengths range. The opposite happens when the background lighting is at the back side (Fig. 3b). Here, the short wavelengths gain increases while the long wavelengths gain decreases. This behavior can be used to build selective filters, where the gain of the short and long pass filters is controlled by optical bias either at the front or back sides.

This nonlinearity allows identifying the different input channels in the visible range. Due to its low wavelength, the background light is absorbed at the top of the front diode and, due to the self-bias effect [6], increases the electric field at the back diode where the red incoming photons are absorbed accordingly their wavelengths (see Fig. 1) resulting in an increased collection. Under back irradiation the electric field decreases mainly at the i-n back interface quenching the red/green input signals.

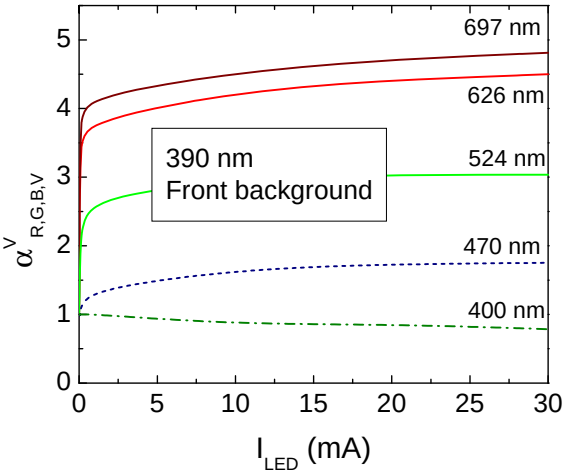

(a)

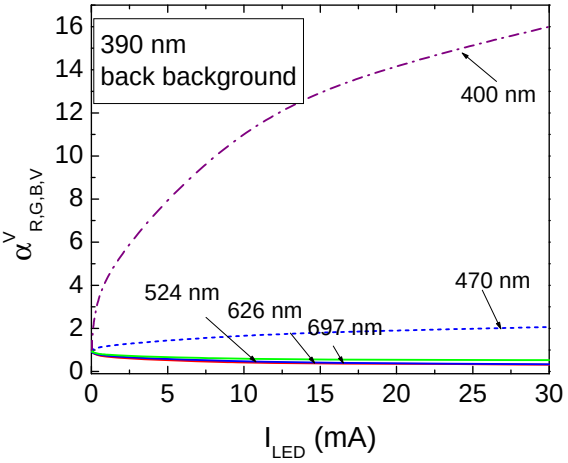

(b)

Fig. 3. (a) front and (b) back optical gain at λ=390 nm irradiation and different input wavelengths.

5. Coder/Decoder Device

In Fig. 4, the normalized MUX signal due to the combination of the red, green, blue and violet input channels (received data) is displayed under front and back irradiations (I_{LED}=30 mA). On the top, the input channels (transmitted data) are displayed. In the right side of the figure all the possible sixteen RGBV sublevels and their 4-bit binary code are inserted.

The results show that to each of all the possible 2^4 *on/off* states it correspond a well-defined level. Under front or back irradiation, each of those four channels, in turn, is enhanced or quenched (Fig. 2 and Fig. 3) accordingly its wavelength. So, 2^4 ordered

levels (d_0-d_{15}) are detected (horizontal dot lines) and grouped into two main classes due to the high amplification of the red channel (α^V_{626}=4.5). The upper eight (2^3) levels are ascribed to the presence of the red channel (R=1), and the lower eight to its absence (R=0), allowing the red channel recognition. Since under front irradiation the green channel is also amplified (α^V_{524}=3) the four (2^2) highest levels, in both classes, are ascribed to the presence of the green channel (G=1) and the four lower ones to its lack (G=0). The blue channel is slightly amplified (α^V_{470}=1.75), so, in each group of 4 entries, two subclasses (2^1) can be found: the two higher levels correspond to the presence of the blue channel (B=1) and the two lowers to its absence (B=0). Finally, each group of 2 entries have two near sublevels (α^V_{400}=0.78), the higher level where the violet channels is ON (V=1) and the lower level where it is missing (V=0).

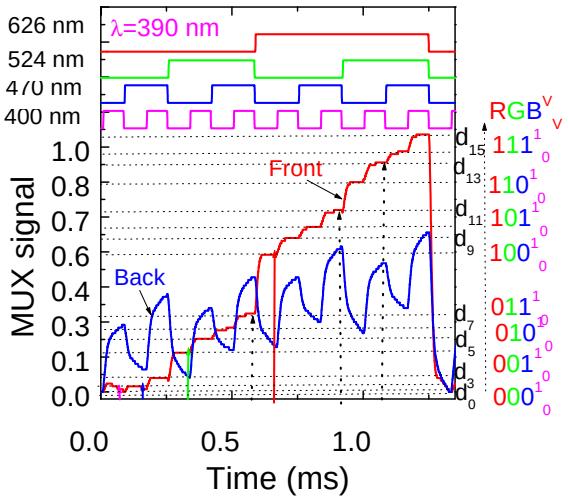

Fig. 4. MUX/DEMUX signals under 390 nm front and back UV irradiation and decoded RGBV binary bit sequences. On the top of the figure the transmitted channels are displayed.

Under back irradiation, the violet channel is strongly enhanced (α^V_{400}=16), the blue channel moderately (α^V_{470}=2) and the green and red strongly reduced ($\alpha^V_{524,626}$=0.3) allowing to confirm the presence of violet channel. In Fig. 4, under front irradiation, d_1 and d_2 have similar values making difficult the decoding; however under back irradiation their recognition is obvious. So, from the front and back information the different bit sequences were decoded and the signal demultiplexed [9].

6. Design of Full-adder Based on a-SiC Technology

A full adder circuit adds three single bit binary numbers (X, Y, Z) and gives result in two single bit binary outputs, called Sum (S) and Carry (C) that is a three-bit modulo-2 addition [12].

A full-adder circuit based on a-SiC technology uses the same principle; it adds three color single bit binary numbers (R, G, B) and gives result in two single bit binary outputs, (Sum, Carry). The design of full adder circuit is illustrated in Fig. 5. Depending upon the state of the variables (R, G, B) the output is obtained from one of the eight output levels (d_0 to d_7).

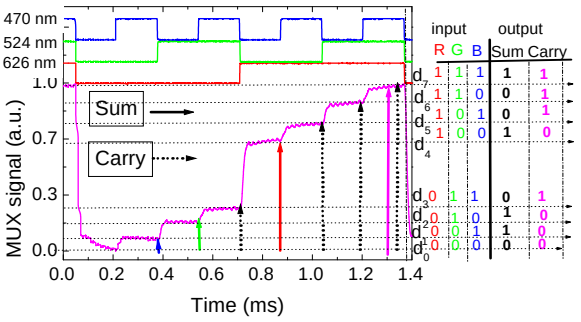

Fig. 5. MUX signal, output levels and truth table of a SiC full adder.

Fig. 5, displays the normalized MUX signals (received data) due to the combination of the red (R), green (G) and blue (B) input channels (transmitted data), under front irradiation. On the top the signals used to drive the input channels are displayed showing the presence of all the possible 2^3 *on/off* states ascribed to 8 separate current levels (d_0-d_7). All eight conditions presented above are listed in Table 1.

Table 1. State of different output levels.

Inputs			Output of the different terminals							
R	G	B	d_0	d_1	d_2	d_3	d_4	d_5	d_6	d_7
0	0	0	1	0	0	0	0	0	0	0
0	0	1	0	1	0	0	0	0	0	0
0	1	0	0	0	1	0	0	0	0	0
0	1	1	0	0	0	1	0	0	0	0
1	0	0	0	0	0	0	1	0	0	0
1	0	1	0	0	0	0	0	1	0	0
1	1	0	0	0	0	0	0	0	1	0
1	1	1	0	0	0	0	0	0	0	1

The corresponding truth table of full adder for three input binary (RGB) variables is shown in the right side of the figure. As expected from Fig. 3 and Fig. 4, the levels magnitude depends on the inputs wavelength amplification factors under irradiation.

So, a 3-binary code is associated to each level allowing signal decoding. Data shows that when one or all of the inputs are present the output will be weighted by their gains ($\alpha^V_{R,G,B}$), which corresponds to four different levels (d_1, d_2, d_4, d_7; solid arrows in

Fig. 5), the system behaves as a XOR gate, i.e., S =1 [13].

If two or three input channels are simultaneously *on*, the output level will be weighted by each of the individual gains, therefore the system acts as AND gate. This corresponds to four separate levels (d_3, d_5, d_6, d_7; dot arrows) and indicates the presence of CARRY bit (C=1).

The truth table of the full-adder shown in the right side of the Fig. 5 is displayed in Table 2.

Table 2. The truth table of the full-adder.

Inputs			Output	
R	G	B	Sum	Carry
0	0	0	0	0
0	0	1	1	0
0	1	0	1	0
0	1	1	0	1
1	0	0	1	0
1	0	1	0	1
1	1	0	0	1
1	1	1	1	1

7. Error Control Based on a-SiC Technology

Fault tolerance can be achieved in many systems by using parity bits. SiC optical processor for error control is realized by using the same double pin/pin a-SiC:H photodetector.

Taking into account Fig. 4, the encoder for code takes four input data bits [R, G, B,V; d_8, d_4, d_2, d_1] and creates three additional parity bits,

$$[P\text{-}(VRG), P\text{-}(VRB), P\text{-}(VGB); d_{13}, d_{11}, d_7], \quad (1)$$

given by:

$$P\text{-}(VRG) = V \oplus R \oplus G, \quad (2)$$

$$P\text{-}(VRB) = V \oplus R \oplus B, \quad (3)$$

$$P\text{-}(VGB) = V \oplus G \oplus B, \quad (4)$$

i.e., the parity bits are SUM bits of the three-bit additions of violet pulsed signal with two additional bits of RGB. So, the seven-bit word at the output of the encoder will be in a bytewide format, with the data and the parity bits separated as decoded in Fig. 4.

Here, the solid arrows shows the different signals that arise from to the presence of one of the four wavelength channels [R, G, B, V] and the doted arrows marks the generate parity bits. Thus, three independent logic functions can be implemented in a SiC WDM circuit. In this case the three-bit adder circuit described above can be used as an encoder for the code, which simultaneously generates the three parity bits. This is schematically shown in Fig. 6.

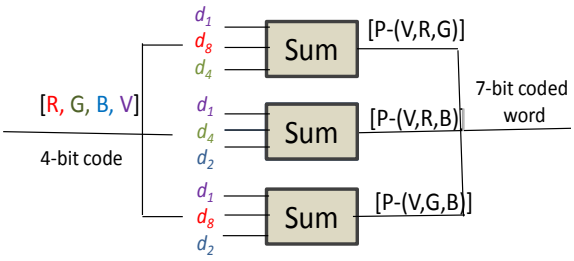

Fig. 6. Schematic of the coding when the three parity bits are generated simultaneously in a SiC WDM circuit.

To make a distinction between transmitted and received data, the transmitted bits are denoted by upper case and the received bits are by lower case. Thus, the transmitted word is:

$$[R, G, B,V, P\text{-}(VRG), P\text{-}(VRB), P\text{-}(VGB)], \quad (5)$$

whereas the received word is:

$$[r, g, b,v, p\text{-}(vrg), p\text{-}(vrb), p\text{-}(vgb)] \quad (6)$$

or else:

$$[d_8, d_4, d_2, d_1, d_{13}, d_{11}, d_7] \quad (7)$$

Since d_1 is present in all three parity bits, it is the first bit that is checked for errors. The following additions are performed on the received bits:

$$v\text{-}(rg) = SUM[p\text{-}(vrg), r,g], \quad (8)$$

$$v\text{-}(gb) = SUM[p\text{-}(vgb),g,b], \quad (9)$$

$$v\text{-}(rb) = SUM[p\text{-}(vrb), r,b] \quad (10)$$

Taking into account Fig. 3b and Fig. 4 under back irradiation, the signal is strongly enhanced if the violet bit is on it *on* state, allowing confirming it presence if generated. Combining the two pieces of information (generated parity bits and back signal levels) either the absence, or the presence of one or double errors, even for similar values of, for instance, d_1 and d_2, will be easily checked.

In the absence of any errors, received bit equals transmitted bit. Each of the above additions would equal d_1. If v-(rg) is computed in the absence of any errors, it equals d_1.

$$v\text{-}(rg) = SUM[p\text{-}(vrg), r,g] = SUM[d_{13}, d_8, d_4] = \\ = d_{13} \oplus d_8 \oplus d_4 = d_1 \oplus d_8 \oplus d_4 \oplus d_8 \oplus d_4 = d_1 \quad (11)$$

In the presence of one error, for example, if the error is on d_2, (see Fig. 4), i.e:

$$\overline{d}_2 = d_2 \oplus 1 \tag{12}$$

and making the same operation:

$$v\text{-}(gb) = SUM[p\text{-}(vgb), g, b), d_4, \overline{d}_2\ ] = d_7 \oplus d_4 \oplus \overline{d}_2 = d_1 \oplus d_2 \oplus 1 \oplus d_4 \oplus d_2 \oplus d_4 = \overline{d}_1 \tag{13}$$

obviously, the results for the two other operations are:

$$v\text{-}(rg) = d_1 \tag{14}$$

and

$$v\text{-}(rb) = \overline{d}_1 \tag{15}$$

However, any double error will not violate the parity check of *P*

$$P = r \oplus g \oplus b \oplus v \oplus p\text{-}(vrg) \oplus p\text{-}(vrb) \oplus p\text{-}(vgb), \tag{16}$$

but will violate some of the p-(vrg), p-(vrb), p-(vgb) parity checks, thus providing an indication of the double error.

Thus, parity preserving reversible circuit design can be implemented optically being very useful in the development of fault tolerant reversible systems in emerging nanotechnology [14].

The way in which the three parity bits are calculated is schematically depicted in Fig. 7. Here, an example of an intuitive representation with the original string color message BRVG; "d_2,d_8,d_1,d_4"="1010" and the transmitted string B R V G; P-(VRB) P-(VRG) P-(VGB) "1010010" is presented (see Fig. 3 and Equation 7).

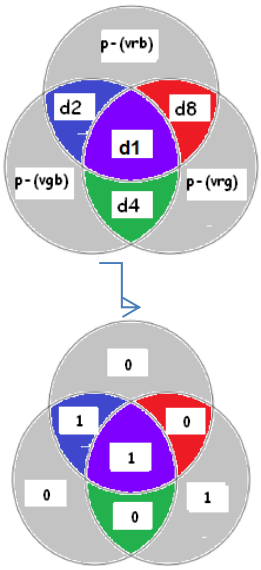

Fig. 7. Example of an intuitive representation with the original string, being the message digits: B R V G "1010" and the transmitted string being B R V G P-(VRB) P-(VRG) P-(VGB) "1010010".

A string of 4 bits is put into this diagram. The parity check bits are set so that the parity within each circle is even (that is, the parity bit is 0 if the sum of the bits in the circle is even and 1 if the sum is odd). This is an intuitive representation of how the parity bits are calculated.

Taking into account Equation 11, in the absence of any errors (Fig. 6), received bit equals transmitted bit. Each of the above additions would equal d_1 confirming:

$$v\text{-}(rg) = v\text{-}(gb) = v\text{-}(rb) = d_1 \tag{17}$$

In Fig. 8a it is displayed the message received d_2 d_8 d_1 d_4 p-(vrb) p-(vrg) p-(vgb) "1**1**10010" with the second bit has likely been altered by noise.

In the presence of one error, for example, if the error is on d_8, by counting 1's in each circle we find that: There is an error in right circle, there is an error in upper circle and there is no error in left circle. Therefore the error is in the second digit, d_8. In agreement with previous conclusions:

$$\text{v-(rg)} = \text{v-(rb)} = \overline{d}_1 \tag{18}$$

$$\text{v-(gb)} = d_1 \tag{19}$$

In Fig. 8b, in the message received d_2 d_8 d_1 d_4 p-(vrb) p-(vrg) p-(vgb) "1**1**1**1**010", the second and fourth bits have likely been altered by noise. Nevertheless, any double error will not violate the parity check of *P* (Equation 16) but will violate some of the p-(vrg), p-(vrb), p-(vgb) parity checks, thus providing an indication of the double error.

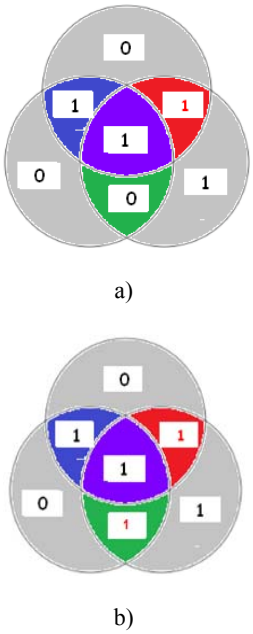

Fig. 8. a) The message received d_2 d_8 d_1 d_4 p-(vrb) p-(vrg) p-(vgb) "1**1**10010" with the second bit has likely been altered by noise, b) The message received d_2 d_8 d_1 d_4 p-(vrb) p-(vrg) p-(vgb) "1**1**1**1**010" with the second and fourth bits have likely been altered by noise.

8. Conclusions

The nonlinear property of the SiC multilayer devices under front and back lighting backgrounds were exploited to design an optical processor for error detection and correction that enables reliable delivery of spectral data of four-wave mixing over unreliable communication channels.

The design of an optical full-adder was presented. Additional parity logic operations were performed using four incoming pulsed communication channels that are transmitted and checked for errors together. As a simple example of this approach, we describe an all optical processor for error detection then provide an experimental demonstration of this idea. An intuitive representation with the original string color message BRVG=“1010” and the transmitted string B R V G; P-(VRB) P-(VRG) P-(VGB) “1010010” is presented.

Acknowledgment

This work was supported by FCT (CTS multi annual funding) through the PIDDAC Program funds and PTDC/EEA-ELC/111854/2009 and PTDC/EEA-ELC/120539/2010.

References

[1]. S. Lin, Y. Ishikawa, K. Wada, Demonstration of optical computing logics based on binary decision diagram, *Optics Express*, 20, 2, 2012, pp. 1378-1384.

[2]. Jin Y. Shen, *et al*., Principles and construction of MSD adder in ternary optical computer, *Sci. China Inf. Sci.*, 53, 2010, pp. 2159–2168.

[3]. R. W. Hamming, Error detecting and error correcting codes, *Bell Syst. Tech. J.*, 29, 1960, pp. 147–160.

[4]. J. Poustie, K. J. Blow, A. E. Kelly, R. J. Manning, All-optical binary half-adder, *Opt. Commun.*, 156, 1998, pp. 22–26.

[5]. K. E. Zoiros, G. Papadopoulos, T. Houbavlis, G. T. Kanellos, Theoretical analysis and performance investigation of ultrafast all-optical Boolean XOR gate with semiconductor optical amplifier-assisted Sagnac interferometer, *Opt. Commun.*, 258, 2, 2006, pp. 114–134.

[6]. T. A. Ibrahim, *et al*., All optical nonlinear switching in GaAs-AlGaAsmicroring resonators, *IEEE Photonics Technology Letters*, 14, 1, 2002, pp. 74-76.

[7]. J. N. Roy, D. K. Gayen, Integrated all-optical logic and arithmetic operations with the help of TOAD based interferometer device – alternative approach, *Appl. Opt*., 46, 22, 2007, pp. 5304–5310.

[8]. M. Vieira, P. Louro, M. Fernandes, M. A. Vieira, A. Fantoni, J. Costa, Three Transducers Embedded into One Single SiC Photodetector: LSP Direct Image Sensor, Optical Amplifier and Demux Device, in Advances in Photodiodes (ed. Gian Franco Dalla Betta), *InTech,* Chap. 19, 2011, pp. 403-425.

[9]. M. A. Vieira, M. Vieira, J. Costa, P. Louro, M. Fernandes, A. Fantoni, Double pin Photodiodes with two Optical Gate Connections for Light Triggering: A capacitive two-phototransistor model, *Sensors & Transducers*, Vol. 9, Special Issue, December 2010, pp. 96-120.

[10]. M. A. Vieira, P. Louro, M. Vieira, A. Fantoni, A. Steiger-Garção, Light-activated amplification in Si-C tandem devices: A capacitive active filter model 2012, *IEEE Sensor Journal*, 12, 6, 2012, pp. 1755-1762.

[11]. M. A. Vieira, M. Vieira, P. Louro, V. Silva, A. S. Garção, Photodetector with integrated optical thin film filters, *Journal of Physics: Conference Series*, 421, 1, March 2013, 012011.

[12]. J. H. Kim, Y. T. Byun, Y. M. Jhon, S. Lee, D. H. Woo, S. H. Kim, All-optical half adder using semiconductor optical amplifier based devices, *Optics Communications*, 218, 2003, pp. 345–349.

[13]. T. Houbavlis, K. E. Zoiros, Ultrafast pattern-operated all-optical Boolean XOR with semiconductor optical amplifer-assisted Sagnac switch, *Opt. Eng*., 42, 12, 2003, pp. 3415–3416.

[14]. M. A. Vieira, M. Vieira, P. Louro, V. Silva, Optical Processor Based on a-SiC Technology for Error Detection on a Spectral Data, in *Proceedings of the 5th International Conference on Sensor Devices, Technologies and Applications (SENSORDEVICES'14),* 16-20 November, Lisbon, Portugal, 2014, pp. 48-53.